Overcoming Endocytosis Deficiency by Cubosome Nanocarriers

Prange, Jenny A ; Aleandri, Simone ; Komisarski, Marek ; Luciani, Alessandro ; Käch, Andres ; Schuh, Claus-Dieter ; Hall, Andrew M ; Mezzenga, Raffaele ; Devuyst, Olivier ; Landau, Ehud M

Abstract: The use of lipid-based nanoparticles for the delivery of biomacromolecules has attracted considerable attention due to the current interest in protein-based therapeutics. Cubosomes protect the incorporated therapeutics, which are susceptible to degradation by enzymes, thereby improving their bioavailability, and concomitantly enhance cellular uptake. The cubosome nanoparticles presented herein were loaded with bovine serum albumin (BSA) and characterized by small-angle X-ray scattering and dynamic light scattering techniques, while the BSA encapsulation and its release were evaluated in vitro. The ability of this formulation to increase the cellular uptake of albumin by 2-fold was tested on various types of renal tubular cells and confirmed by in vivo renal uptake experiments in mice. The obtained results show that cubosomes are able to deliver BSA inside the cell through distinct uptake and intracellular routing. These data were substantiated, with evidence of a high cubosome-mediated uptake of BSA in Clcn5 knockout mice characterized by defective receptor-mediated endocytosis. The use of cubosomes as a delivery system thus represents a promising approach to overcome the low endocytic uptake in diseased epithelial cells and to treat dysfunctions of the kidney proximal tubule.

DOI: https://doi.org/10.1021/acsabm.9b00187

Originally published at:
Prange, Jenny A; Aleandri, Simone; Komisarski, Marek; Luciani, Alessandro; Käch, Andres; Schuh, Claus-Dieter; Hall, Andrew M; Mezzenga, Raffaele; Devuyst, Olivier; Landau, Ehud M (2019). Overcoming Endocytosis Deficiency by Cubosome Nanocarriers. ACS Applied Bio Materials, 2(6):2490-2499.
DOI: https://doi.org/10.1021/acsabm.9b00187

Overcoming Endocytosis Deficiency by Cubosome Nanocarriers

Jenny A. Prange[1*], Simone Aleandri[2*], Marek Komisarski[2], Alessandro Luciani[1], Andres Kaech[3], Claus-Dieter Schuh[4], Andrew M Hall[4], Raffaele Mezzenga[5], Olivier Devuyst[1**], Ehud M. Landau[2**]

[1]Institute of Physiology, University of Zurich, Zurich

[2]Department of Chemistry, University of Zurich, Zurich

[3]Center for Microscopy and Image Analysis, University of Zurich

[4]Institute of Anatomy, University of Zurich, Zurich

[5]Department of Health Sciences & Technology, ETH Zurich

*JAP and SA: co-first authors

**OD and EML: co-last authors, co-directed the study

ABSTRACT

The use of lipid-based nanoparticles for the delivery of bio-macromolecules has attracted considerable attention due to the current interest in protein-based therapeutics. Cubosomes protect the incorporated therapeutics, which are susceptible to degradation by enzymes, thereby improving their bioavailability, and concomitantly enhance cellular uptake. The cubosome nanoparticles presented herein were loaded with bovine serum albumin (BSA), and characterized by small angle X-ray scattering and dynamic light scattering techniques, while the BSA encapsulation and its release were evaluated *in vitro*. The ability of this formulation to increase by two fold the cellular uptake of low-molecular-weight (LMW) tracers was tested on various types of renal tubular cells, and confirmed by in *vivo* renal uptake experiments in mice. Obtained results show that cubosomes are able to deliver BSA inside the cell through a distinct intracellular routing. Even in state of genetically-driven disruption of receptor mediated endocytosis, the BSA uptake is increased irrespective of the genetic background and its degradation in lysosomes delayed. These data were substantiated *in vivo*, with evidence of high cubosome-mediated uptake of BSA in wildtype mice and in *Clcn5*$^{y/-}$ mice characterized by defective receptor-mediated endocytosis.

The use of cubosomes as a delivery system able to overcome the low endocytic uptake in diseased epithelial cells thus represents a promising approach to treat proximal tubule dysfunctions.

INTRODUCTION

An ideal drug delivery system (DDS) should be stable and biocompatible, incorporate the active agent without loss or alteration of its activity, provide an efficient delivery to specific location *in vivo*, and also show optimal cellular uptake and clearance pathways, thereby enhancing the *in vivo* efficiency of the drug [1, 2]. Cellular uptake and efficient release at its target location are the first challenges to consider when designing nanocarriers as DDS. The nanoparticle can enter the cell via an endocytic pathway; however the endocytosed nanoparticles should be able to escape endosomal entrapment before formation of acidic late endosomes in addition to resist clearance via endocytic recycling and exocytosis [3]. Controlling endosomal release is therefore crucial in the design of nanoparticles for efficient drug delivery.

The size and the shape of nanoparticles are critical factors to control cellular uptake [4]. Specifically, for lipid-based nanoparticles, the membrane properties and the particle's internal structure have a key role in cellular drug delivery efficiency [5]. Lipidic mesophases (LMPs) composed by monoolein (MO) show a higher endosomal escape, precisely the escape from late endosomes to avoid lysosomal degradation, in mammalian cell culture when compared to parent Lipoplex systems [6]. The LMP's membrane is able to efficiently escape from endosomal entrapment by lowering the free energy cost of forming pores in endosomal membranes. LMPs are similar in consistency and rheology to cross-linked polymeric hydrogels. However, these bulk phases that lack colloidal stability are not suitable in a systemic administration that requires a stable nanoscale particulate system.

Cubosomes, the water-dispersed form of the lipidic cubic phase, possess an identical microstructure to that of the parent gel phase, but exhibit a much lower viscosity in comparison to the bulk phase [7]. Such dispersions are commonly prepared by mixing monoolein (MO) and water in appropriate proportions, and are stabilized by using a poly (ethylene oxide) −poly (propylene oxide) −poly (ethylene oxide) block copolymer [8]. Compared with the parent gels, dispersions exhibit improved fluidity and larger surface area, thereby providing various means of potential formulations [9]. The use of cubosomes for the delivery of bio-macromolecules has attracted considerable attention due to the current interest in protein-based therapeutics [10, 11]. Many studies have shown that the thermal stability and activity of proteins are retained within a cubic phase matrix. Moreover, the structure of lipidic cubic phase represents an ideal medium for the encapsulation of soluble and integral membrane proteins ranging in size from lysozyme (14 kDa [12]) to fibrinogen (340 kDa [13]).

The epithelial cells lining the proximal tubules (PT) of the kidney constitute a paradigm of effective communication between the external environment and the endomembrane system, allowing to reabsorb a large amount of filtered ions and solutes. By processing incoming substances and recycling receptors and transporters at the apical plasma membrane, the connecting endolysosomal system dictates the terminal differentiation of the cells, and hence the recovery and processing of essential substances that would otherwise be lost in the urine [14]. In particular, the reabsorption of albumin and low-molecular-weight (LMW) proteins from the glomerular filtrate occurs via receptor-mediated endocytosis in PT cells. This process is initiated by the binding of ligands to the receptors megalin and cubilin, followed by their internalization through clathrin-coated pits and processing in the endolysosomes [15]. In genetic and acquired kidney disorders this process is disrupted, causing massive loss of solutes in the urine resulting in life-threatening complications [16-19]. A paradigm of defective receptor-mediated endocytosis is Dent disease, caused by inactivating mutations in the *CLCN5* gene coding for the endosomal chloride-proton exchanger ClC-5. Investigations using the well-established *Clcn5* knock-out mouse model of Dent disease have demonstrated that the disease is caused by a generalized trafficking defect, with loss of apical megalin and cubilin receptors, leading to the massive urinary loss of albumin and LMW solutes [14, 16]. The uptake of albumin and LMW tracers is routinely investigated in various cellular systems modelizing PT cells, characterized by variable levels of differentiation and endocytic uptake capacity [20].

The goal of this study was to probe the potential of cubosome nanoparticles as a biocompatible and non-toxic delivery system to overcome the deficient receptor-mediated endocytic activity in the renal proximal tubule. Colloidally stable cubosome nanoparticles composed of MO and loaded with labeled bovine serum albumin (BSA) are presented in this study. The cubosomes were characterized by small angle X-ray scattering and dynamic light scattering techniques. The uptake of the cubosome-BSA formulation was tested *in vitro* on different PT cell models and confirmed by in *vivo* experiments in *Clcn5* mice. These data constitute the first *in vivo* application of cubosomes, which are able to overcome a clinically-relevant defect in endocytosis.

EXPERIMENTAL SECTION

Chemicals and reagents

1-Monooleoyl-*sn*-glycerol C18: 1 (monoolein, MO) was purchased from Nu-Chek Prep, Inc. (MN, USA), phosphate buffer solution (PBS (1X) pH 7.4), BSA from Bovine Serum (BSA) Alexa Fluor® 488 conjugate and BSA Alexa Fluor® 647 conjugate were purchased from Invitrogen. Pluronic® F-127 (PF127), BSA was purchased from Sigma Aldrich. All solutions were prepared using Mill-Q water (18.2MΩ cm^{-1}; Millipore, Bedford, MA). Conjugate BSA-Gold 10nm was purchased from BBI™ solutions (Cardiff, UK).

Preparation of cubosomes

Cubosomes (empty, loaded with BSA Alexa Fluor® 488 conjugate, BSA Alexa Fluor® 647 conjugate, Conjugate BSA-Gold or BSA) were prepared as described by Murgia *et al.* [21]. Briefly, a solution of the appropriate amount of MO in $CHCl_3$ was evaporated to provide a film of MO on the wall of a round-bottom flask. A solution of stabilizer (PF127) in PT cell medium was added to the preformed films after overnight storage in a desiccator under reduced pressure (0.4 mbar) to yield the cubosome solution with the desired lipid concentration. The solution was vortex-mixed and then dispersed using an ultrasonic processor Brenson digital 250 (cycle 0.9s on/ 0.9s off, amplitude 50%, for 10min). Subsequently, the cubosome dispersion was filtered through Acrodisc 450nm. The concentrations of MO and stabilizer in the resulting dispersions were typically 0.150mg/mL and 0,0136mg/mL, respectively. For the BSA-loaded cubosomes, an aliquot of BSA solution in PBS (5mg/mL) was added to a vial with dry MO in order to obtain the appropriate amount of BSA after hydration. The lipid and protein mixture was then processed as described previously.

Dynamic light scattering (DLS)

Particle size and z-potential determination of the cubosomes were performed immediately after preparation, and one week later (while the aggregate size was checked every day) with a Zeta Sizer Nano ZS (Malvern Instruments, Malvern, UK) at 37 ± 0.1°C. The samples were housed in disposable polystyrene cuvettes of 1 cm optical path length with water as solvent. Scattering angle was 90°. At least three independent samples were taken, each of which was measured between three to five times. The width of the DLS hydrodynamic diameter distribution is indicated by PDI (polydispersion index). The intensity size distribution of the

cubosomes was typically unimodal; therefore the autocorrelation function was analyzed according to the cumulant method.

Small angle X-ray scattering (SAXS)

SAXS measurements were used to determine the symmetry and unit cell dimensions of the cubosomes (33mg/mL MO and 0.3mg/mL PF127) under various conditions. Experiments were performed either on the empty cubosomes or on the loaded cubosomes (the molar ratio of BSA to lipid is 1:280, which is identical to the ratio used in the experiments with the cells) using a microfocused Rigaku X-ray source of wavelength $\lambda = 1.54$Å, operating at 45kV and 88 mA. Scattered X-ray signal was detected with a gas-filled two-dimensional (2D) detector. The scattering vector $q = (4\pi/\lambda)\sin\theta$, with 2θ being the scattering angle, was calibrated using silver behenate. The sample-to-detector distance was 1m, providing a q range from 0.005 to 0.77Å^{-1}. Data were collected and azimuthally averaged using the Saxsgui software to yield 1D intensity versus scattering vector q. Samples were loaded into a quartz glass capillary (Hiligenberg, length: 80mm; outside: 2.0mm; wall thickness: 0.01mm). Measurements were performed at 37°C, and samples were equilibrated for 10min prior to measurements, while scattered intensity was collected over 10 hours. A mathematical model was used to calculate the structural parameter of the *Im3m* phases. Briefly, following determination of the lattice parameter by SAXS, and assuming a fixed lipid volume fraction, and a constant geometry of the *Im3m* system, the aqueous channel diameter (D_w) was calculated according to Meli *et al.*[22].

Dialysis

Excess non-incorporated BSA (BSA Alexa Fluor® 488 conjugate, and BSA Alexa Fluor® 647 conjugate and Gold-BSA) were separated from the cubosomes by dialysis as follows: About 5mL of sample was placed in the Spectra/Por membrane (300KDa cut off; Spectrum Laboratories Inc., USA) and dialyzed against water (500mL) for 48h at 25°C. The encapsulation efficiency (E%) of BSA (BSA Alexa Fluor® 488 conjugate, and BSA Alexa Fluor® 647 conjugate) entrapped in cubosomes after dialysis was established by spectrofluorometry (with Infinite® 200 Tecan) and calculated using equation **1**. The amount of BSA (in mg/mL) entrapment in the formulation was determined by using a calibration curve.

$$E\ (\%) = F_{after} / F_{before} \times 100\% \qquad \text{Eq. 1}$$

Where F_{before} and F_{after} are the fluorescence values of BSA in the cubosomes before and after dialysis.

The amount of BSA (BSA Alexa Fluor® 488 conjugate, and BSA Alexa Fluor® 647 conjugate and Conjugate BSA-Gold 10nm) entrapped in cubosomes after the dialysis was additionally confirmed by a standard Pierce™ BCA protein assay (Thermo Fisher, Scientific).

Release experiments

Following removal of the free (un-entrapped) protein, the cubosomes were transferred to a new dialysis tube at 7 consecutive time points (after 1, 2, 3, 4, 5, 6 and 7 days). Immediately before loading the sample into the tube (T_0), an aliquot of cubosomes (100 mL) was removed from the dialysis tube and analyzed spectrofluorimetrically. All measurements were performed at 37°C. The percentage of Alexa Fluor® BSA release was determined by equation **2** and plotted versus time.

$$\% \text{ Release} = 100 - (F_t / F_0 \times 100) \qquad \text{Eq. 2}$$

Where F_t and F_0 are the values of fluorescence at times t and 0, respectively, *i.e.* before loading the sample.

Fluorescence quenching experiments

Fluorescence quenching experiments on a solution of BSA dissolved in PBS, and on BSA entrapped in cubosomes were performed before and after dialysis treatment using iodide (I^-) as collisional quencher. All fluorescence experiments were carried out at 37°C on solutions with optical densities smaller than 0.05 to minimize inner filter effects. Fluorescence quenching experiments were performed by adding small aliquots of 0.1 M I^- (containing small amount of $Na_2S_2O_4$ to avoid the oxidation of the quencher) solution to the samples [23]. The concentrations of the lipid and BSA were 0.150mg/mL and 0.1mg/mL, respectively. Decrease of the fluorescence of the BSA Alexa Fluor® 488 conjugate was monitored at 526nm by exciting at 480nm.

Fluorescence anisotropy

Fluorescence Anisotropy experiments on a solution of the BSA Alexa Fluor® 488 conjugate dissolved in PBS or entrapped in cubosomes, before and after dialysis treatment were

performed. Anisotropy measurements were collected using an L-format configuration, and all data were corrected for polarization bias using the G-factor. Low-volume quartz cuvettes with an optical path length of 1.0 × 0.2cm were used to reduce the scattering effects from the cubosome solutions. The concentration of the MO and BSA were 0.150mg/ mL and 0.1mg/ mL respectively.

Proximal tubule cell types and culture conditions

Immortalized human kidney cells, HK2 (ATCC, Teddington, UK) were cultured in endothelial growth medium (DMEM F-12, 21041-025, Life technology) supplemented with EGM single quots (Lonza, CC-4133). The immortalized opossum kidney, OK, cells (ATCC, Teddington, UK) were cultured in DMEM (Gibco; Life Technologies, Paisley, UK) containing 10% FCS (Gibco; Life Technologies, Paisley, UK). Cells were grown on chamber slides (Falcon, VWR) or 96 well plates until confluent [20].

Differentiated, polarized mouse primary PT cells were obtained after micro-dissection of mouse kidney cortex and cultured as previously described [17].

MTT assay (Cell Counting Kit-8, Dojindo Laboratories, Kumamoto, Japan).

Cells were seeded on 96-well cell culture plates (Nunc, Thermo Scientific, Roskilde, Denmark) and treated with Cyclohexylamine (CHA, Sigma-Aldrich, Steinheim, DE) once they were confluent. After incubation with CHA, 10µl of CCK-8 solution (Dojindo Laboratories, Kumamoto, Japan) was added to the well and incubated for 4h at 37°C. Subsequently, the absorbance at 450nm was determined using an Infinite M200 Pro TECAN spectrophotometer (Tecan, Männedorf, Switzerland). Equal numbers of untreated cells were used as controls [20].

Cubosome treatment *in vitro*. Cells were grown until confluent and then starved with serum-free medium to reduce background signal through maintenance turnover. The cells were pulsed with cubosome solution for 1h at 4°C. Three different sample preparations were used: pure Alexa Fluor® BSA (0.1mg/ml), pure Alexa Fluor® BSA (0.1mg/ml) mixed with empty cubosomes (150µg/ml) and with cubosomes (150µg/ml) loaded with Alexa Fluor® BSA (0.1mg/ml), respectively to directly compare the influence of the cubosome nanoparticles on the endocytic process.

Time course experiment and inhibition. Cells were grown until confluent and subsequently starved with serum-free medium to reduce background signal through maintenance turnover. Confluent chamber slides were then pulsed with cubosome samples for 1h at 4°C, with subsequent degradation monitored at t=0, 5min, 15min, 60min. Metabolic inhibition was achieved by 10mM NaN_3/ 50mM DOG (Sigma) and lysosomal block was obtained using 250mM Bafilomycin respectively [17]. For both inhibitions the agents remained in the medium through the whole process.

Immunostaining. After cubosome incubation, cells were fixed for 10min at -20°C in ice-cold methanol (Methanol purum, UZH, Zurich, Switzerland). After 3x5min washing in PBS, 30min blocking at room temperature was performed in PBS (Gibco; Life Technologies, 14040-091) supplemented with 5%FBS and 1% Triton-X-100 (Sigma Aldrich, Steinheim, DE, 9284). Incubation with primary antibodies, diluted in antibody dilution buffer (PBS, 1% BSA (VWR, 421501J), 1% Triton-X-100) was done for 2-3h at room temperature. The cells were then washed 3x5min in PBS and incubated with secondary antibody (diluted 1:200 in antibody dilution buffer) for 1h at room temperature in the dark. After 3x5min washing in PBS, the slides were mounted with ProLong® Gold with Dapi (Life Technologies) and stored at 4°C until analysis.
The following antibodies were used for immunostaining: Rab5 (Abcam, ab18211), Rab7 (Abcam, ab137029), CatD (Santa Cruz, sc-7486).

Microscopy.
Confocal Microscopy: CLSM Leica SP5 Mid UV-VIS/ resonant. Picture processing and analysis was done using Imaris Software 7.6.3.
Electron microscopy. 150µg/ml cubosomes were loaded with 100 µg/ml BSA-gold and incubated for 1h at 37°C on confluent cells. Cells were then first fixed with 2.5% glutaraldehyde (Sigma Aldrich) in 0.1M cacodylate buffer for 1 hour at 37°C and sequentially treated with 1% OsO_4 for 1 hour at 0°C and 2% uranyl acetate in nanopure water for 1h at 4°C. The cells were dehydrated in an ethanol series and embedded in Epon/Araldite (Sigma-Aldrich). Ultrathin (50 nm) sections were contrasted with lead citrate and examined with a CM100 transmission electron microscope (FEI, Eindhoven, The Netherlands) at an acceleration voltage of 80 kV using an Orius 1000 digital camera (Gatan, Munich, Germany).

Cubosome treatment *in vivo*.

Experiments were conducted on male knock-out (*Clcn5*$^{Y/-}$) and wild-type (*Clcn5*$^{Y/+}$) littermates (C57BL/6 background [16]). Mice were maintained under temperature-and humidity-controlled conditions with 12-h light/12-h dark cycles with free access to appropriate standard diet in accordance with the institutional guidelines of National Institutes of Health Guide for the Care and Use of Laboratory Animals. The protocols were approved by the Animal Ethics Committees of the University of Zurich.

Mice (*Clcn5*$^{Y/-}$ vs. wild-type) were anaesthetized with inhaled isoflurane (Attane, Provet AG, Switzerland) in 100 ml/min Oxygen. For dye application the internal jugular vein was cannulated (PE10 tubing), the left kidney was externalized for imaging and the mouse was mounted on a custom-built temperature-controlled holder specially designed to reduce movement artefacts. Imaging was performed on a custom-built microscope as described by Mayrhofer [24] and Schuh [25]. 250µl of the cubosome or control solution (both containing 0.1mg/ml BSA) was injected with a 500µl Hamilton glass syringe (model 1750TLLX, Hamilton) at a rate of 300 µl/minute. Imaging was performed at a rate of 1 frame/10 sec. After frame 6 (1 min) the automated syringe pump (pump 11 elite nanomite, Havard apparatus) was activated. For the time series analysed a total of 80 frames were recorded, the intensity changes were analysed in FIJI (imageJ). For general analysis ROI squares (15 x 15px) were placed on the nephron or the vasculature. As raw data 32 signal positive nephron segments (PTs) were chosen (only 19 in CLC5 BSA since not more positive nephron segments found), their mean intensity over time (80 fr) was exported to excel 2013 and the mean +/- SEM was visualized with graphpad prism. The images for Fig. 6 were exported as single frame after 11 min recording with Imaris (Bitplane, vs. 7.7.2). The resolution is 1024 x 1024px and all images were adjusted to the settings (minimum 0, maximum 2500 & gamma 1). The images were exported as grayscale in 12 bit with 600 dpi (tiff) and the movie files were generated with Imaris and recorded as avi with 1024 x 1024 px, no compression and 10 frames per second.

Statistical analysis

Data were expressed as mean ± SEM. Significance of differences was assessed by unpaired Student t-test. P values < 0.05 were considered statistically significant.

RESULTS

Characterization of the cubosome aggregates

The final concentrations of MO and PF127 in the cubosome dispersions were typically 0.150 and 0.0136 mg/mL, respectively. SAXS experiments were performed on empty and BSA-loaded cubosomes (Table 1; Fig.1A).

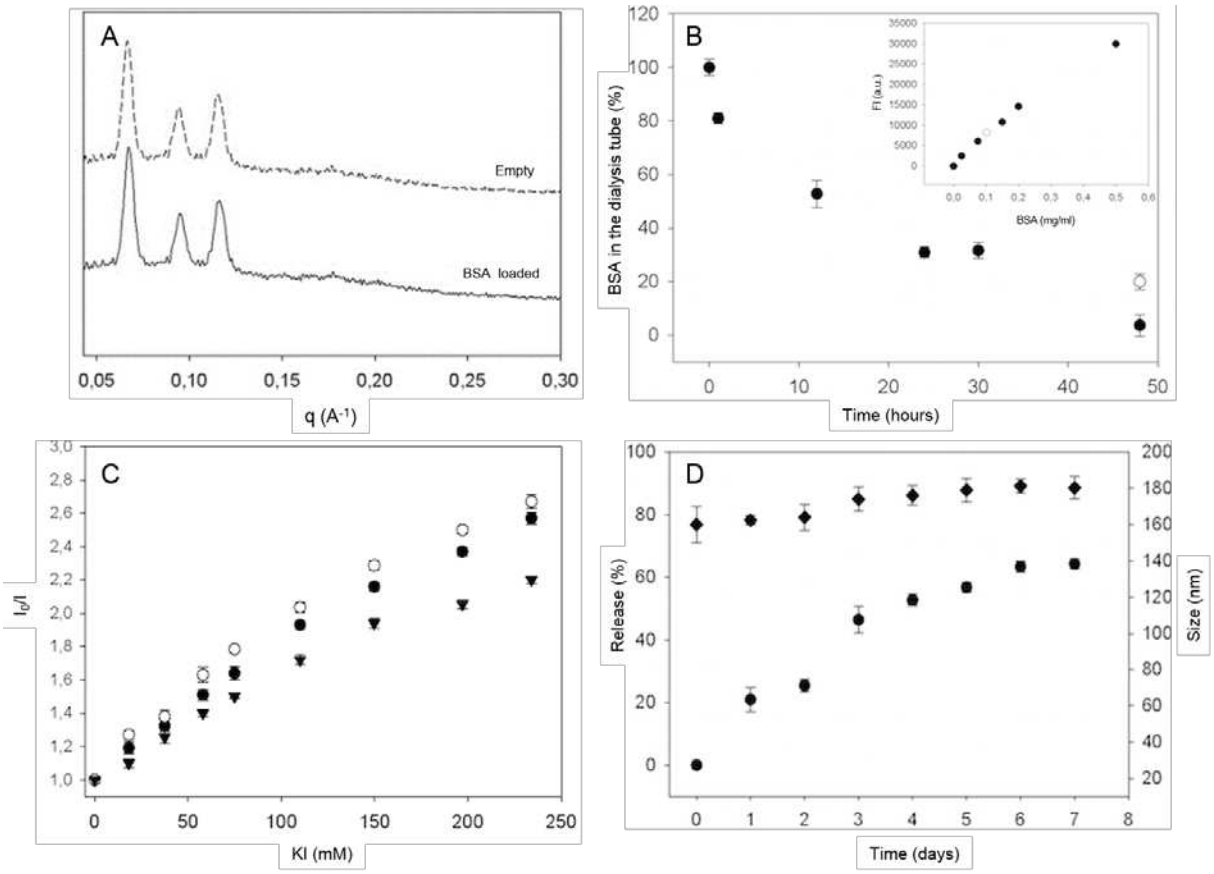

Figure 1. Cubosome preparation
(A) SAXS spectra of empty and BSA-loaded cubosomes. (B) % of BSA in the dialysis tube plotted versus time. BSA solution in PBS, and BSA loaded in cubosomes are shown as black and white circles, respectively. The inset shows the calibration curve of BSA Alexa Fluor® 488 conjugate (black circles) and the amount of BSA Alexa Fluor® 488 conjugate in cubosomes after dialysis (white circle). Data are expressed as mean ± SD from three independent experiments. (C) Fluorescence quenching experiments by I- of: BSA solution in PBS (white circles), BSA incorporated in cubosomes before and after dialysis treatment (black circles and triangles, respectively). Mean ± SD (n=3). (D) Percentages of BSA release (black circles) from the aqueous compartments of the cubosomes as a function of time (left axis) and size measurement (black diamonds, right axis) as a function of time. Mean ± SD (n=3).

Table 1*. Samples, mean diameter (Dav), Polydispersity index (PDI), ζ-potential (z-pot), phase identity (P.I), crystallographic unit cell parameters (a) and water channel diameter (dw) observed for the cubosome nanoparticles.*

Sample	D_{av} (nm)	PDI	ζ-pot (mV)	P.I.	a (Å)	d_w (Å)
Empty	139 ± 4	0.08±0.01	- 25.8 ± 0.5	*Im3m*	135.4	48,8
BSA-Loaded	142 ± 2	0.09 ± 0.02	- 26.0 ± 0.4	*Im3m*	134.8	48,4

MO dispersions in PF127 constitute a well-known system, and the phase diagram of the ternary MO/water/PF127 system is reported [26]. In agreement with the literature, addition of PF127 to the system induces a cubic-*Pn3m* to cubic-*Im3m* phase transition [27]. Interestingly,

addition of the soluble protein BSA, at the level used, does not affect the phase identity and the lattice parameter (see Table 1) of the MO/H_2O/PF127 system [5, 28], which is *Im3m* throughout, with a unit cell parameter of 134.8 Å. The cubosomes used in this study - empty and loaded with BSA - show larger aqueous channel diameters (48.8 Å and 48.4 Å, respectively) as compared with cubosomes of *Pn3m* symmetry [22], whose aqueous channel diameters range in size between 35 and 40 Å [21]. Moreover, as summarized in Table 1, incorporation of the BSA does not alter the size and the z-potential of the aggregates [29].

Efficacy of BSA entrapment

Excess of non-incorporated BSA was removed from the cubosomes by dialysis as reported in the experimental section. The amount of BSA loaded in cubosomes after the dialysis was analyzed spectrofluorimetrically and determined using a calibration curve. When a BSA solution in PBS (0.5 mg/mL) was loaded into the dialysis tube, the entire protein content can diffuse trough the membrane tube, and hence no protein was detected in the tube after 48 hours (black circles Fig. 1B). In contrast, when BSA (0.5 mg/mL) is incorporated in the cubosomes, 20 % of the protein (white circle Fig. 1B), corresponding to 0.1 mg/mL of BSA are firmly entrapped in the cubosome after the same dialysis treatment (marked as a white circle in the inset of Fig. 1B). The amount of BSA loaded in the cubosomes was also confirmed by protein quantification assay, as described in the experimental section.

Location of BSA and release from cubosome structures

Fluorescence anisotropy and quenching measurements provide independent confirmation that BSA is embedded in the aqueous channels of the cubosome. Solutions of BSA Alexa Fluor® 488 dissolved in PBS, and BSA Alexa Fluor® 488 entrapped in cubosomes (final concentration of BSA is 0.1 mg/mL) were subjected to fluorescent anisotropy experiments. The anisotropy values of BSA are 0.06 ± 0.005 and 0.15 ± 0.002 for the free and BSA loaded cubosomes, respectively. Moreover, fluorescence quenching measurements of BSA included in cubosomes (dialyzed sample, black triangles in Fig. 1C) clearly show a decrease of the BSA quenching. The protein is therefore less accessible to the quencher when compared to the un-dialyzed and free protein samples (black and white circles, respectively in Fig. 1C). BSA release from cubosomes was subsequently investigated by fluorescence experiments as discussed above. As shown in Fig. 1D (black circles; left axis) only about 22 % BSA was released up to 2 days, and a slow release occurs within one week (60 % of the loaded BSA). Furthermore, the size of cubosomes does not increase during the release, as shown in Fig. 1D

(diamonds, right axis), confirming that the protein is able to diffuse out from the aqueous channels of the cubosomes without aggregation.

Assessment of cubosome toxicity on human kidney cells

The potential toxicity of empty cubosomes as function of concentration and incubation time was evaluated using the standard MTT assay for cell viability on HK2 cells, which are routinely used for PT cell toxicology screening. A significant decrease in cell viability was observed after 1h incubation with empty cubosomes of concentrations of 200µg/ml (viability 25 ± 13.7%) and 500µg/ml (4 ± 4%), whereas viability was not significantly affected at concentrations of 100µg/ml and 150µg/ml (viability 97 ± 3% and 84 ± 3%, respectively) (Table 2; Suppl. Fig. 1A).

Table 2. *Viability of HK2 cells after incubation with various concentrations of empty cubosomes for 1h at 37°C.*

	Cubosome concentration (µg/ml)				
	0	100	150	200	500
Viability (%)	100 ± 2.6	97 ± 2.6	84 ± 2.9	25 ± 13.7 ***	3.7 ± 4.1 ***

3 wells per condition in 3 independent experiments. *** *$p<0.001$ compared to control (0)*

A time-course experiment with empty cubosomes exhibiting the highest-tested concentration that did not have significant impact on cell viability (150 µg/ml) did not show any significant changes in cell viability upon exposure up to 60 min (Table 3).

Table 3. *Viability of HK2 cells after time course incubation with 150µg/ml cubosomes loaded with 0.1mg/ml BSA.*

	Incubation time (min)			
	0	5	15	60
Viability (%)	100 ± 2.6	94 ± 1.6	95 ± 1.3	92 ± 0.7

3 wells per condition in 3 independent experiments. No significant differences.

As BSA can slowly diffuse out of the cubic phase, the effective BSA concentration was independently confirmed using a standard BCA protein quantification kit (Suppl. Fig. 1B). Based on the results obtained in the experiments above, a final working cubosome concentration of 150 µg/ml, loaded with 100µg/ml BSA (to avoid cell overloading) was established and used for all experiments, unless otherwise indicated.

Uptake and processing of BSA-loaded cubosomes in low-endocytic capacity cells

Initially, the internalization and degradation of BSA-loaded cubosomes in HK2 cells, characterized by a relatively low endocytic capacity [20], was monitored. Following a pulse of 1h at 4°C, the localization of BSA was analyzed at different time points by confocal microscopy (Fig. 2A) and the Alexa Fluor® 488 BSA signal was quantified using a fluorescence plate reader (Fig. 2B).

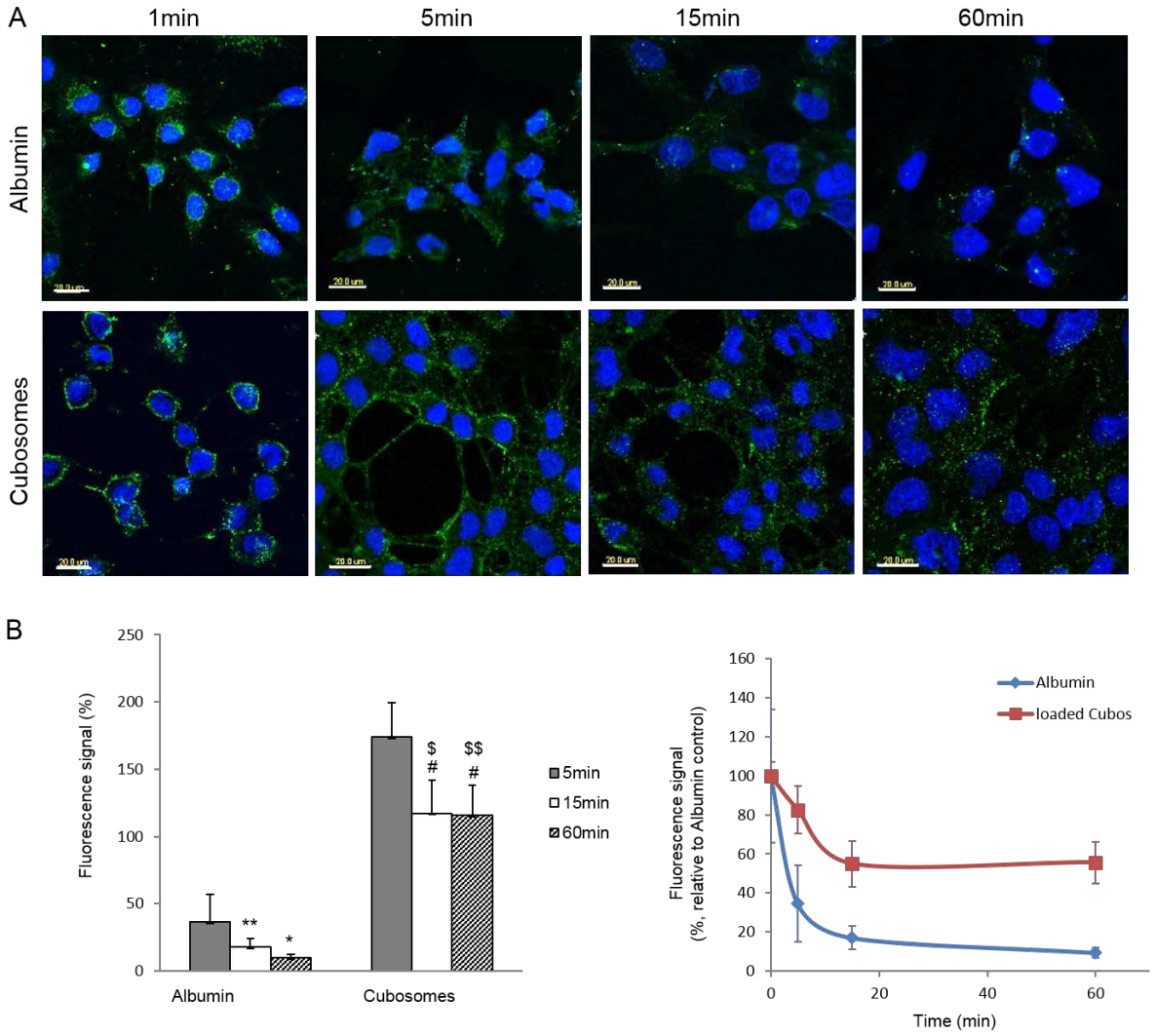

Figure 2. BSA degradation in HK2 cell monolayers
*HK2 cells were cultured on chamber slides, pulsed with 0.1mg/ml Alexa Fluor® BSA for 1h at 4°C, either pure or loaded in 0.15mg/ml cubosomes, and degradation was monitored (A) for the indicated time points. Fluorescence signal of pure BSA is cleared after 60min degradation while the BSA signal from cubosomes remains strong. (B) After cell lysis, fluorescence signal for indicated time points was quantified relative to the Albumin control, presented in %. Significant decrease of fluorescence signal could be observed for both conditions (BSA and cubosomes) after 30 and 60min. Cubosomes show a significantly stronger signal at all times compared to pure BSA. *# p<0.05, ** p<0.01, ### p<0.001 with * vs. control and # vs. Albumin.*

Exposure of HK2 cells to Alexa Fluor® 488-BSA alone led to rapid internalization followed by sizeable degradation already at 15 min and an almost complete loss of signal after 1h (Fig. 2A upper row). The same incubation with Alexa Fluor® 488-BSA loaded into cubosomes resulted in a much stronger fluorescence signal which could be detected up to 60 min after the pulse (Fig. 2A, lower row). These observations were supported by the quantification of the residual signal of Alexa-488 BSA (Fig. 2B; Table 4).

Table 4*. Impact of empty cubosomes on endocytosis in HK2 cells (%) after incubation with either pure bovine serum albumin (BSA, 0.1mg/ml), BSA co-incubated with empty (0.15mg/ml) cubosomes (BSA+Cubos), or 0.1mg/ml BSA loaded into 0.15mg/ml cubosomes (Cubos).*

	5min	**15min**	**60min**
BSA	36 ± 20	18 ± 6**	9 ± 3*
BSA+Cubos	42 ± 1	32 ± 21	15 ± 8

loaded Cubos	173 ± 25$^{\$}$	115 ± 25$^{\#, \$}$	117 ± 23$^{\#, \$\$}$

3 wells per condition in 3 independent experiments. $^{*\#\$}p<0.05$, $^{**\$\$}p<0.01$
(*BSA vs control, $^{\#}$ cubosomes vs control, $^{\$}$ BSA vs. cubosomes, BSA+Cubos vs. BSA not significant

A significant decrease of the internalized BSA was already observed after 15min, whereas only approximately 10% of residual signal was detected after 1 hour. In contrast, the initial signal obtained for Alexa Fluor® 488-BSA-loaded cubosome incubation was 4-fold increased (173 ± 25%, $p<0.05$) compared to the pure Alexa Fluor® 488-BSA uptake (36 ± 20%). Despite a decrease after 15min and 60min, a significant residual signal persisted at 1 hour, amounting to a 10-fold higher intensity than that obtained for Alexa Fluor® 488-BSA alone. Confocal Z-stack analysis confirmed the internalization of the Alexa Fluor® 488-BSA cargo in HK2 cells (data not shown).

To rule out the possibility that the presence of cubosomes *per se* might affect the endocytic uptake, the uptake in HK2 cells of Alexa Fluor® 488-BSA alone (0.1 mg/ml) or combined with empty cubosomes was compared. The presence of empty cubosomes did not affect the uptake of BSA in these monolayers, and the signal was significantly decreased after 60 min in both conditions (Suppl. Fig. 2).

Table 5*. Analysis of co-localization (%) of BSA with endo-lysosomal markers (Rab5, Rab7, CatD) after incubation of HK2 cells with either pure BSA (0.1mg/ml, BSA) or BSA loaded into 0.15mg/ml cubosomes (Cubos).*

Incubation	**15 min**	**60 min**	
Marker	**Rab5**	**Rab7**	**CatD**
BSA	72 ± 3.2	20.5 ± 1.6	56.9 ± 4
Cubos	48.8 ± 2.7 **	70.4 ± 3.6 ***	19.5 ± 2.5 ***

All cells of 5 images per staining in 3 independent experiments. $^{**}p<0.01$, $^{***}p<0.001$ vs. control.

Immunofluorescent staining with endo-lysosomal markers (Fig. 3; Table 5) substantiated the co-localization of internalized Alexa Fluor® 488-BSA in Rab5-positive early endosomes (72 ± 3%) after 15min, and with cathepsin D-positive lysosomes (57 ± 4%) and the late endosomal marker Rab7 (21 ± 2%) after 60min (Fig. 3A upper row).

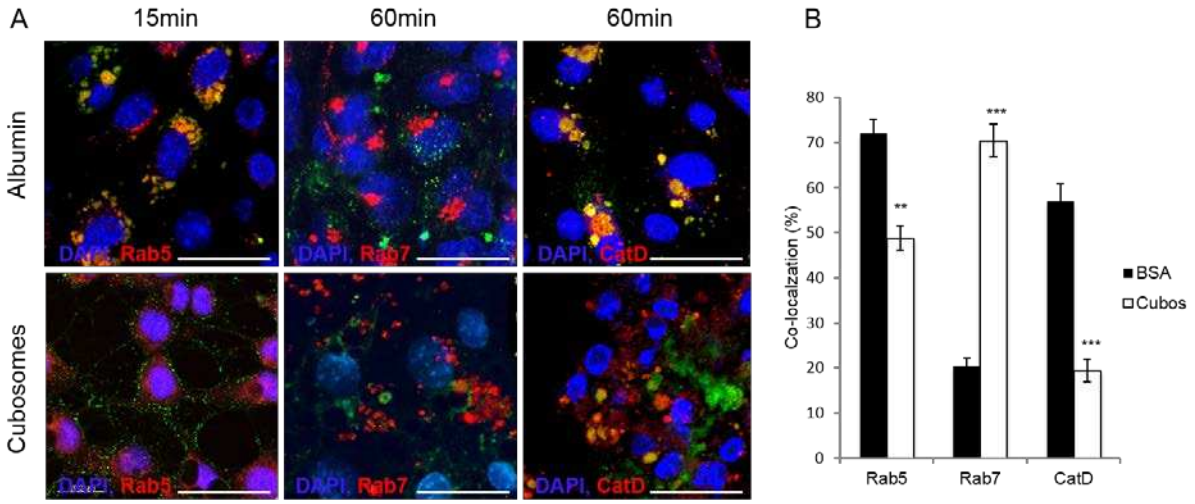

Figure 3. Intracellular localizalion of BSA
*Bafilomycin treated, methanol fixed monolayers were stained for endosomal (Rab5, Rab7) and lysosomal markers (CatD). (A) Confocal analysis shows co-localization between pure BSA and both markers (Rab5, CatD) after 15 resp. 60min degradation, while cubosomes do only co-localize partially with Rab7 and CatD after 60min. (scale bar 25µm) (B) Colocalization analysis shows a shift of cubosome signal towards the late endosomes after 60min when naturally BSA is already found in the degrading lysosomes. ** p<0.01, ***p<0.001 BSA vs Cubosomes at corresponding time points.*

In contrast, Alexa Fluor® 488-BSA delivered within cubosomes showed some co-localization (49 ± 3%) with early endosomes after 15min, and a robust co-localization (70 ± 4%) with late endosomes contrasting with a lower signal (20 ± 3%) with lysosomes after 60 min (Fig. 3A lower row).

Taken together, these data suggest that, compared with direct incubation of BSA alone, delivery of BSA within cubosomes is manifested by a higher uptake, a distinct intracellular routing and a delayed degradation in HK2 cells.

Subcellular distribution of BSA

Electron microscopy was used to substantiate the subcellular distribution of gold-labelled BSA in HK2 cells (Fig. 4).

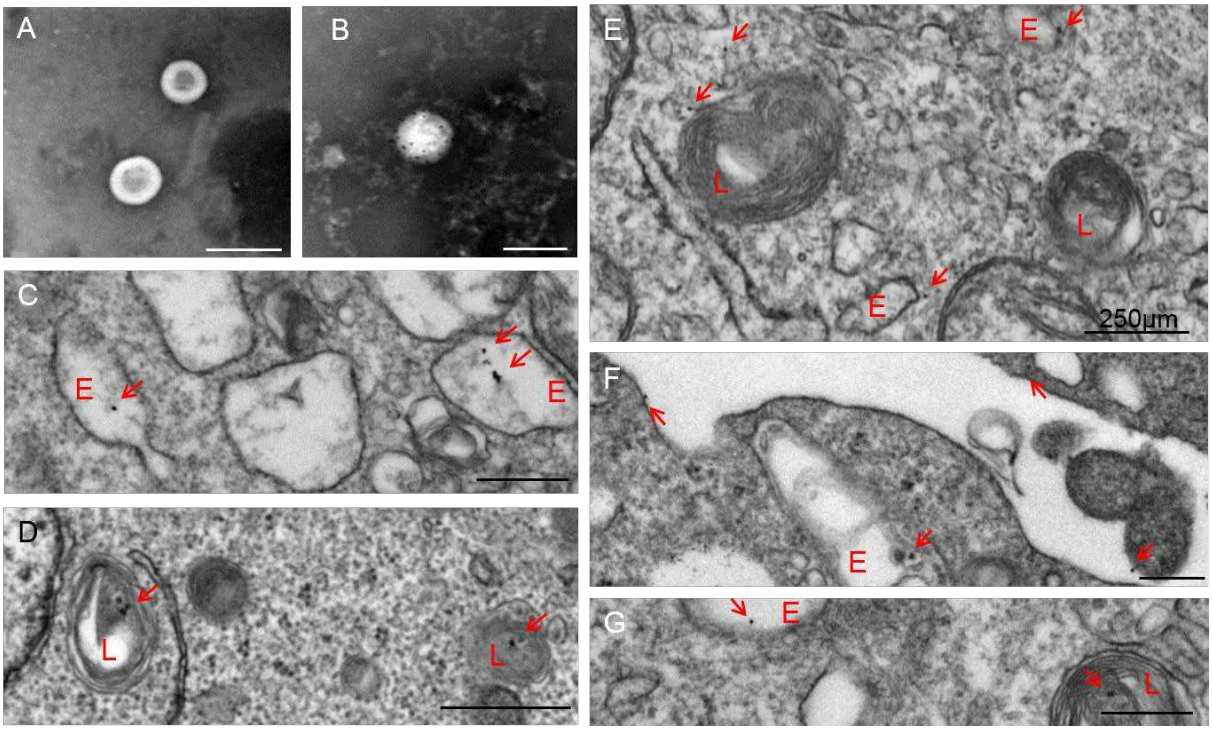

Figure 4. EM Analysis after incubation with cubosomes loaded with BSA-gold
Further localization analysis was performed using transmission electron microscopy with GA-fixed cell pellets. (A) Empty cubosome, (B) BSA-Gold loaded cubosome. The localization of pure BSA-Gold particles in endosomes (C) as well as lysosomes (D) was shown. However, Cubosomes loaded with BSA-Gold were mostly found intracellularly (E, Scale bar 250µm) and started to show in endosome-like structures after 60min. (E, F scale bar 500µm)

Empty cubosomes and cubosomes loaded with Alexa Fluor® 488-BSA were first detected separately and extracellularly for technical adjustments, as shown on representative images in Fig. 4 A/B. Under standard conditions (incubation of HK2 cells with pure BSA-gold), BSA was detected after 5 min in endosomes (simple membrane-surrounded structures; Fig. 4C), and after 60 min in lysosomes (multi-layered structures; Fig. 4D). Following incubation with cubosomes containing gold-labelled BSA, the gold particles were mostly detected free in the cytosol after 5 min (Fig. 4E) and rarely in the lysosomes, but rather in the endosomes after 60 min (Fig. 4F-G). While endosomes show a simple membrane structure, lysosomes can be distinctively identified through their characteristic multi-layered membranes (Fig. 4C-G). These observations support the distinct processing and subcellular localization of the cargo internalized through cubosomes.

Uptake and processing of BSA-loaded cubosomes in OK cells

In order to assess the potential effect of the variable endocytic rate at baseline, we performed similar uptake experiments in OK cells, which are characterized by a high basal level of receptor-mediated endocytosis (Prange, 2016). The OK cell monolayers were incubated with either Alexa Fluor® 488-BSA (100 µg/ml) alone or with BSA loaded into 150 µg/ml cubosomes (Suppl. Fig 3A/B; Table 6).

Table 6. *Comparison of the impact of 0.15mg/ml cubosomes on endocytosis of 0.1mg/ml BSA (ng/µg protein) in different cell lines: low endocytic cell line (HK2), high endocytic cell line (OK) and primary cells from different genetic backgrounds. Values are normalized to 15min time point of HK2.*

Cell line	Substrate	Time point (min)	Uptake (% rel. to HK2)
HK2	**BSA**	**15**	100.00 ± 26.67
		60	14.09 ± 3.71 **
	Cubos	**15**	185.18 ± 15.28 $^{\#}$
		60	48.95 ± 20.56 *
OK	**BSA**	**15**	185.84 ± 0.37
		60	33.69 ± 4.25 ***
	Cubos	**15**	198.91 ± 35.45
		60	118.04 ± 9.39 $^{\#\#, *}$
mPTC *Clcn5* WT	**BSA**	**15**	665.42 ± 56.1
		60	260.25 ± 21.55 *
	Cubos	**15**	1597.2 ± 68.99 $^{\#\#\#}$
		60	407.45 ± 61.49 **
mPTC *Clcn5* KO	**BSA**	**15**	405.6 ± 53.13
		60	190.69 ± 10.34 **
	Cubos	**15**	1571.7 ± 267.57 $^{\#\#}$
		60	351.49 ± 71.26 **

3 wells per condition in 3 independent experiments. $^{*\#}$ p<0.05, $^{**\#\#}$ p<0.01, $^{***\#\#\#}$ p<0.001 with * compared to 15min and $^{\#}$ BSA vs cubos.

Representative images are shown in Fig. 3A.The initial uptake values (15 min) of pure BSA vs. BSA loaded cubosomes are similar in OK cells (1.07 fold increase from BSA to cubosomes), contrasting with the almost doubled uptake for BSA in cubosomes observed in the HK2 cells (185 ± 15% uptake with cubosomes, relative to BSA). However, after 60 min, the degradation of BSA in cubosomes is similarly reduced under control conditions (albumin degradation) in OK (63.5 ± 5%) as it is in HK cells (49 ± 21%). Furthermore, albumin levels remain significantly increased after 60min with cubosome treatment compared to the albumin treatment to the same extend within the OK cell line as is the case for the HK2 cell line (Suppl. Fig. 3B; Table 6). In comparison to both, an increase can be observed for the incubation with cubosomes compared to BSA in mouse primary cells (mPTC) for both wildtype (2-fold) and KO (3-fold) after 15min (240 ± 10% for WT, resp. 236 ± 40% for KO). The later time point did not reveal any significant difference between WT and KO ($p > 0.05$).

Uptake and processing of BSA-loaded cubosomes in proximal tubule cells and intact kidneys from *Clcn5* mice

The experiments performed in different cell systems indicated a distinct intracellular routing and delayed degradation when using cubosomes to deliver BSA in PT cells. In order to test the potential relevance for such delivery in clinical situations, we conducted experiments using the *Clnc5* KO model, a faithful model of Dent disease characterized by defective receptor-mediated endocytosis causing a generalized loss of solutes in the urine [14, 16].
The uptake of pure Alexa Fluor® 488-BSA and of BSA in cubosomes was compared in highly differentiated mPTCs obtained from *Clcn5* KO and WT kidneys (Fig. 5, Table 6).

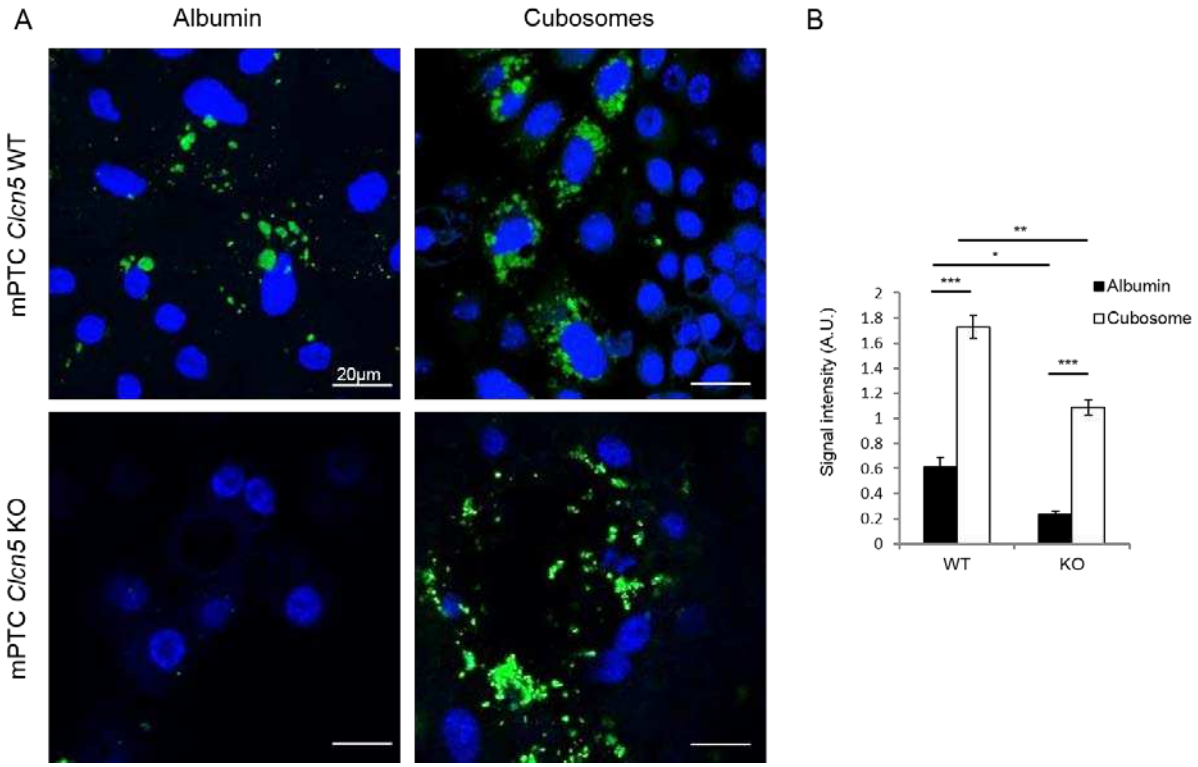

Figure 5. Application of cubosomes in an endocytosis-deficient cell model
*Self-dissected primary PT cells were generated and grown to monolayers as previously described [30]. The clcn5 KO mouse model was used as an endocytosis-deficient model and compared to WT. Monolayers were incubated with either 0.1mg/ml pure Alexa-488 BSA or 0.15mg/ml cubosomes containing 0.1mg/ml Alexa-488 BSA for 15min. Uptake was monitored (scale bar 20µm, A) and quantified (B). Clcn5 deficient cells show a clear decrease in the uptake of pure BSA compared to WT cells, but the application of cubosomes seems to overcome this deficiency and restores the uptake. * p<0.05, ** p<0.01, ***p<0.001*

As expected, the uptake of 0.1mg/ml pure BSA was significantly reduced in the *Clcn5* KO as compared with WT mPTCs (405± 53% vs. 665 ± 56%., respectively, $p < 0.05$). The delivery of BSA in cubosomes enhanced the uptake in both conditions, with a 2.5-fold increase in WT cells vs a 4-fold increase in KO cells (Suppl. Fig. 3B). Importantly, the delivery of BSA with cubosomes enabled to increase the albumin uptake of KO cells up to the same level as that observed for WT cells (1577 ± 67% resp. to 1571 ± 268%).
Intravital multiphoton microscopy has emerged in the last decade as a powerful tool to study dynamic physiological processes *in vivo*. With this technique it is possible to follow the filtration, uptake and handling of solutes in real time in the intact kidney [25]. To assess the

handling of cubosomes *in vivo* they were injected through a jugular vein catheter into either WT or *clcn5*$^{y/-}$ mice while simultaneously imaging the kidney outer cortex (Suppl. videos). As can be seen in the videos, BSA was visible in the vasculature immediately post-injection, and after 20 seconds it appeared in the PT brush border, consistent with rapid filtration. Shortly afterwards, BSA signal was localized to PT endosomes, and then subsequently to lysosomes. Quantification of signal intensity over time revealed that uptake of cubosome-BSA was strikingly higher than with BSA alone (approximately 10 fold higher) (Fig. 6A/B).

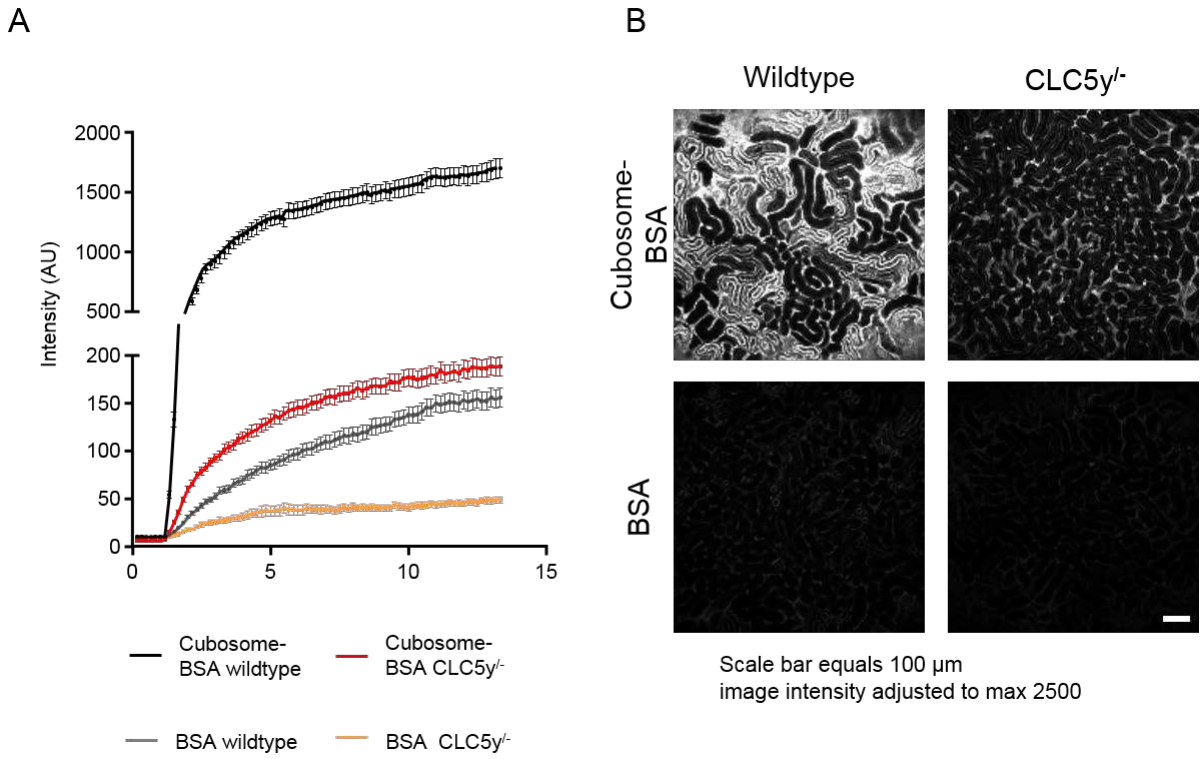

Figure 6. In vivo uptake quantification.
250µl of 0.1mg/ml pure fluorescently-labeled BSA or 0.15mg/ml cubosome solution (containing 0.1mg/ml fluorescently-labeled BSA) was injected via a cannulated internal jugular vein into WT and clcn5 KO mice. The left kidney was externalized and real-time imaging performed with multiphoton microscopy. (A) Quantification of fluorescent BSA signal intensity in proximal tubules over time revealed that uptake was much higher when injected in cubosomes, compared to BSA alone, in both wildtype and CLC5$^{y/-}$ *mice. The uptake of BSA in cubosomes in CLC5*$^{y/-}$ *mice even exceeded that in wildtype mice injected with BSA alone. (B) Representative images are depicted of BSA uptake 10 minutes post-injection (scale bar = 100 µm).*

As expected, uptake of BSA alone was much lower in *clcn5*$^{y/-}$ mice. However, uptake of cubosome-BSA was substantially increased in both animals, WT and KO, and final signal intensities of cubosome-BSA treated KO animals were even higher than those of BSA alone in WT mice. To confirm the uptake of cubosome-BSA into lysosomes, mice were co-injected with the established lysosomal fluorescent marker Lysotracker, which was observed to co-localize with the BSA signal (Suppl. Fig 4).

DISCUSSION

The utilization of cubosomes as protein carriers requires a comprehensive understanding and control of their physico-chemical properties. In this investigation, empty cubosomes, as well as cubosomes loaded with BSA were prepared following a state-of-the-art, bottom-up approach [21]. SAXS was used to systematically investigate the particle design space of MO-based cubic structure.

Cubosomes can generally entrap proteins [13, 31, 32] and release them after a certain time [33]. The encapsulation efficiency depends on the method of preparation used, on the lipid type and the concentration [9, 13]. In our approach, following dialysis treatment of the formulation, 20 % of the protein, corresponding to 0.1 mg/mL of BSA is stably entrapped in the cubosome. The location of the protein in the aqueous channels of the cubosomes was determined by anisotropy and quenching fluorescence measurements. Fluorescence quenching was used to obtain information about the position of the fluorophore in the lipid bilayer by studying the accessibility of the quencher (I^-) to the fluorophore and the efficiency of quenching [34]. Fluorescence measurements clearly show a decrease of the quenching of the protein: BSA in the dialyzed sample is therefore located in the aqueous channels of the cubosomes, and the fraction of BSA accessible to the quencher decreases. Moreover, an increase of the anisotropy value confirms that the protein is located in a structure with a reduced mobility [21].

As discussed above, cubosomes are able to entrap BSA and prevent its spontaneous burst release with time. Small drugs are known to release virtually immediately from cubosomes [35] by virtue of the high surface area-to-volume ratio of submicron particles However, BSA, being a relatively large and somewhat surface active protein appears to be retained in the cubosomes for a period of days, slowly leaking from the matrix into the surrounding solution. The release behavior therefore confirms the ability of cubosomes to entrap the protein and avoid its fast release.

We used various types of PT cell systems to investigate the potential toxicity of the cubosomes and to monitor the internalization and intracellular distribution of the cargo at the light and electron microscopy levels. The handling of BSA-loaded monoolein-based cubosomes was tested on well-established renal PT cells, characterized by variable levels of differentiation ranging from HK2 cells (low endocytic activity), OK cells (intermediate endocytic activity) and mPTC (primary cultures, high endocytic activity [20]). The effective working concentration (0.15mg/ml cubosomes carrying 0.1mg/ml Alexa Fluor® 488-BSA) did not affect cell viability and corresponded to the maximal amount of BSA technically possible to load into the cubosomes (part of the originally loaded BSA diffuses out of the

cubic phase during the production). Hence, the concentration of albumin within the cubosome solution is slightly below the physiological one (2.7 - 3.5 mg/dl) but leaves room for technical optimization depending on the particular cargo.

Pulse-chase experiments in PT cells showed delayed degradation of the Alexa Fluor® 488-BSA signal when applied in cubosomes, compared with incubation with BSA alone. A possible explanation might be that cubosomes bypass the endocytic receptors responsible for the uptake and subsequently internalization and processing in the endolysosome compartment. No specific binding of the cubosomes to the megalin receptor is expected: even after short incubation, no membrane associated fluorescence signal could be observed with the cubosomes. The pathways potentially involved in cubosome internalization include channels and other, non-receptor mediated forms of endocytosis such as pinocytosis or phagocytosis.

We observed that cubosomes are able to increase the uptake of BSA in HK2 cells and mPTCs but not in OK cells. Reasons for these differences may include variable differentiation levels in the cells, resulting in low expression levels of receptors and/or transport systems located in the apical membrane [20].

Confirmation that BSA-loaded cubosomes are taken up and processed in the endo-lysosomal compartment was provided by z-stack analysis, TEM and co-localization studies with endolysosomal markers in PT cells. Compared to pure BSA, which mostly co-localized under Bafilomycin-treated conditions in early endosomes after 15 min, only very few endosomes co-localized with cubosome-delivered BSA at this stage. While pure BSA was mostly located into lysosomes (marker:Rab7 and CatD) at 60min, only minimal colocalization was obtained for cubosome delivered BSA. These differences could be due to the distinct entry pathway(s) of cubosomes - bypassing the receptors and the potential re-arrangement of cubosome lipids into the cellular membranes upon entry into the cell. The cubosome membrane shape is by itself active, lowering the free energy required to promote fusion and pore formation with the endosomal membrane and leading to an efficient escape [5]. Hence, one might describe this observation as endosomal escape [36], which could be further supported by the fact that metabolic inhibition as well as lysosomal blocking with Bafilomycin did not affect the degradation of Alexa Fluor® 488-BSA when delivered within the cubosomes. Further studies with tagged lipid entities would be needed to substantiate that hypothesis.

Since the cubosomes appear to bypass the megalin and cubilin receptors for PT cell internalization, they could be used to internalize cargo in genetic disorders affecting receptor-mediated endocytosis. The latter hypothesis was tested *in vitro* and *in vivo*, using the described mouse model of Dent's disease – an example of defective endocytosis. Whereas the

uptake of BSA alone was much lower in *clcn5*$^{y/-}$ primary cells and mice, as expected, the uptake of cubosome-BSA was increased in both cases, and was even higher than that of BSA alone in WT mice. These data support that cubosomes present a potent new system to deliver cargo across cell membranes, even when endocytic receptors are genetically deficient.

In summary, the results presented support the use of cubosomes as a delivery system able to overcome the low endocytic uptake in diseased epithelial cells. They represent a promising approach to treat proximal tubule dysfunctions and, more generally, defects in highly reabsorptive epithelial cells.

REFERENCES

1. Zabara, A.; Mezzenga, R., Controlling molecular transport and sustained drug release in lipid-based liquid crystalline mesophases. *J Control Release* **2014,** *188*, 31-43.
2. Maeda, H.; Sawa, T.; Konno, T., Mechanism of tumor-targeted delivery of macromolecular drugs, including the EPR effect in solid tumor and clinical overview of the prototype polymeric drug SMANCS. *J Control Release* **2001,** *74* (1-3), 47-61.
3. Sahay, G.; Querbes, W.; Alabi, C.; Eltoukhy, A.; Sarkar, S.; Zurenko, C.; Karagiannis, E.; Love, K.; Chen, D.; Zoncu, R.; Buganim, Y.; Schroeder, A.; Langer, R.; Anderson, D. G., Efficiency of siRNA delivery by lipid nanoparticles is limited by endocytic recycling. *Nat Biotechnol* **2013,** *31* (7), 653-8.
4. Barua, S.; Mitragotri, S., Challenges associated with Penetration of Nanoparticles across Cell and Tissue Barriers: A Review of Current Status and Future Prospects. *Nano Today* **2014,** *9* (2), 223-243.
5. Kim, H.; Leal, C., Cuboplexes: Topologically Active siRNA Delivery. *ACS Nano* **2015,** *9* (10), 10214-26.
6. Leal, C.; Ewert, K. K.; Shirazi, R. S.; Bouxsein, N. F.; Safinya, C. R., Nanogyroids incorporating multivalent lipids: enhanced membrane charge density and pore forming ability for gene silencing. *Langmuir* **2011,** *27* (12), 7691-7.
7. Lynch, M. L. S., P. T., *Bicontinuous Liquid Crystals*. 1 ed.; CRC Press: 2005.
8. Kaasgaard, T.; Drummond, C. J., Ordered 2-D and 3-D nanostructured amphiphile self-assembly materials stable in excess solvent. *Phys Chem Chem Phys* **2006,** *8* (43), 4957-75.
9. Hartnett, T. E.; O'Connor, A. J.; Ladewig, K., Cubosomes and other potential ocular drug delivery vehicles for macromolecular therapeutics. *Expert Opin Drug Deliv* **2015,** *12* (9), 1513-26.
10. Dimitrov, D. S., Therapeutic proteins. *Methods Mol Biol* **2012,** *899*, 1-26.
11. Leader, B.; Baca, Q. J.; Golan, D. E., Protein therapeutics: a summary and pharmacological classification. *Nat Rev Drug Discov* **2008,** *7* (1), 21-39.
12. Zabara, A.; Amar-Yuli, I.; Mezzenga, R., Tuning in-meso-crystallized lysozyme polymorphism by lyotropic liquid crystal symmetry. *Langmuir* **2011,** *27* (10), 6418-25.
13. Angelov, B.; Angelova, A.; Mutafchieva, R.; Lesieur, S.; Vainio, U.; Garamus, V. M.; Jensen, G. V.; Pedersen, J. S., SAXS investigation of a cubic to a sponge (L3) phase transition in self-assembled lipid nanocarriers. *Phys Chem Chem Phys* **2011,** *13* (8), 3073-81.
14. Devuyst, O.; Luciani, A., Chloride transporters and receptor-mediated endocytosis in the renal proximal tubule. *J Physiol* **2015,** *593* (18), 4151-64.
15. Christensen, E. I.; Birn, H.; Storm, T.; Weyer, K.; Nielsen, R., Endocytic receptors in the renal proximal tubule. *Physiology (Bethesda)* **2012,** *27* (4), 223-36.
16. Christensen, E. I.; Devuyst, O.; Dom, G.; Nielsen, R.; Van der Smissen, P.; Verroust, P.; Leruth, M.; Guggino, W. B.; Courtoy, P. J., Loss of chloride channel ClC-5 impairs endocytosis by defective trafficking of megalin and cubilin in kidney proximal tubules. *Proc Natl Acad Sci U S A* **2003,** *100* (14), 8472-7.
17. Luciani, A.; Sirac, C.; Terryn, S.; Javaugue, V.; Prange, J. A.; Bender, S.; Bonaud, A.; Cogne, M.; Aucouturier, P.; Ronco, P.; Bridoux, F.; Devuyst, O., Impaired Lysosomal Function Underlies Monoclonal Light Chain-Associated Renal Fanconi Syndrome. *J Am Soc Nephrol* **2016,** *27* (7), 2049-61.
18. Raggi, C.; Luciani, A.; Nevo, N.; Antignac, C.; Terryn, S.; Devuyst, O., Dedifferentiation and aberrations of the endolysosomal compartment characterize the early stage of nephropathic cystinosis. *Hum Mol Genet* **2014,** *23* (9), 2266-78.

19. Terryn, S.; Tanaka, K.; Lengele, J. P.; Olinger, E.; Dubois-Laforgue, D.; Garbay, S.; Kozyraki, R.; Van Der Smissen, P.; Christensen, E. I.; Courtoy, P. J.; Bellanne-Chantelot, C.; Timsit, J.; Pontoglio, M.; Devuyst, O., Tubular proteinuria in patients with HNF1alpha mutations: HNF1alpha drives endocytosis in the proximal tubule. *Kidney Int* **2016,** *89* (5), 1075-1089.
20. Prange, J. A.; Bieri, M.; Segerer, S.; Burger, C.; Kaech, A.; Moritz, W.; Devuyst, O., Human proximal tubule cells form functional microtissues. *Pflugers Arch* **2016,** *468* (4), 739-50.
21. Murgia, S.; Bonacchi, S.; Falchi, A. M.; Lampis, S.; Lippolis, V.; Meli, V.; Monduzzi, M.; Prodi, L.; Schmidt, J.; Talmon, Y.; Caltagirone, C., Drug-loaded fluorescent cubosomes: versatile nanoparticles for potential theranostic applications. *Langmuir* **2013,** *29* (22), 6673-9.
22. Meli, V.; Caltagirone, C.; Falchi, A. M.; Hyde, S. T.; Lippolis, V.; Monduzzi, M.; Obiols-Rabasa, M.; Rosa, A.; Schmidt, J.; Talmon, Y.; Murgia, S., Docetaxel-Loaded Fluorescent Liquid-Crystalline Nanoparticles for Cancer Theranostics. *Langmuir* **2015,** *31* (35), 9566-75.
23. Pownall, H. J.; Smith, L. C., Fluorescence quenching of anthracene in charged micelles by pyridinium and iodide ions. *Biochemistry* **1974,** *13* (12), 2594-7.
24. Mayrhofer, J. M.; Haiss, F.; Haenni, D.; Weber, S.; Zuend, M.; Barrett, M. J.; Ferrari, K. D.; Maechler, P.; Saab, A. S.; Stobart, J. L.; Wyss, M. T.; Johannssen, H.; Osswald, H.; Palmer, L. M.; Revol, V.; Schuh, C. D.; Urban, C.; Hall, A.; Larkum, M. E.; Rutz-Innerhofer, E.; Zeilhofer, H. U.; Ziegler, U.; Weber, B., Design and performance of an ultra-flexible two-photon microscope for in vivo research. *Biomed Opt Express* **2015,** *6* (11), 4228-37.
25. Schuh, C. D.; Haenni, D.; Craigie, E.; Ziegler, U.; Weber, B.; Devuyst, O.; Hall, A. M., Long wavelength multiphoton excitation is advantageous for intravital kidney imaging. *Kidney Int* **2016,** *89* (3), 712-9.
26. Landh, T., Phase Behavior in the System Pine Needle Oil Monoglycerides-Poloxamer 407-Water at 20.degree. *J Phys Chem* **1994**.
27. Dong, Y. D.; Larson, I.; Hanley, T.; Boyd, B. J., Bulk and dispersed aqueous phase behavior of phytantriol: effect of vitamin E acetate and F127 polymer on liquid crystal nanostructure. *Langmuir* **2006,** *22* (23), 9512-8.
28. Yang, J., Stimuli-responsive drug delivery systems. *Adv Drug Deliv Rev* **2012,** *64* (11), 965-6.
29. Barauskas, J.; Johnsson, M.; Joabsson, F.; Tiberg, F., Cubic phase nanoparticles (Cubosome): principles for controlling size, structure, and stability. *Langmuir* **2005,** *21* (6), 2569-77.
30. Terryn, S.; Jouret, F.; Vandenabeele, F.; Smolders, I.; Moreels, M.; Devuyst, O.; Steels, P.; Van Kerkhove, E., A primary culture of mouse proximal tubular cells, established on collagen-coated membranes. *Am J Physiol Renal Physiol* **2007,** *293* (2), F476-85.
31. Svensson, O.; Thuresson, K.; Arnebrant, T., Interactions between chitosan-modified particles and mucin-coated surfaces. *J Colloid Interface Sci* **2008,** *325* (2), 346-50.
32. Yang, Z. P., X.; Tan, Y.; Chen, M.; Zhu, X.; Feng, M.; Xu, Y.; Wu, C., Optimization of the Preparation Process for an Oral Phytantriol-Based Amphotericin B Cubosomes. *Journal of Nanomaterials* **2011,** *2011*.
33. Rizwan, S. B.; Assmus, D.; Boehnke, A.; Hanley, T.; Boyd, B. J.; Rades, T.; Hook, S., Preparation of phytantriol cubosomes by solvent precursor dilution for the delivery of protein vaccines. *Eur J Pharm Biopharm* **2011,** *79* (1), 15-22.

34. Bombelli, C.; Stringaro, A.; Borocci, S.; Bozzuto, G.; Colone, M.; Giansanti, L.; Sgambato, R.; Toccaceli, L.; Mancini, G.; Molinari, A., Efficiency of liposomes in the delivery of a photosensitizer controlled by the stereochemistry of a gemini surfactant component. *Mol Pharm* **2010,** *7* (1), 130-7.
35. Boyd, B. J.; Khoo, S. M.; Whittaker, D. V.; Davey, G.; Porter, C. J., A lipid-based liquid crystalline matrix that provides sustained release and enhanced oral bioavailability for a model poorly water soluble drug in rats. *Int J Pharm* **2007,** *340* (1-2), 52-60.
36. Varkouhi, A. K.; Scholte, M.; Storm, G.; Haisma, H. J., Endosomal escape pathways for delivery of biologicals. *J Control Release* **2011,** *151* (3), 220-8.